

## Heterolytic H<sub>2</sub> Activation Mediated by Low-Coordinate L<sub>3</sub>Fe-(μ-N)-FeL<sub>3</sub> Complexes to Generate Fe(μ-NH)(μ-H)Fe Species

Steven D. Brown, Mark P. Mehn, and Jonas C. Peters\*

Division of Chemistry and Chemical Engineering, Arnold and Mabel Beckman Laboratories of Chemical Synthesis, California Institute of Technology, Pasadena, California 91125

Received July 5, 2005; E-mail: jpeters@caltech.edu

Recently, we described the characterization of an unusual bimetallic bridged iron nitride,  $\{([\text{PhBP}_3]\text{Fe})_2(\mu\text{-N})\}^-$ , distinct by virtue of the low coordination number (CN = 4) and oxidation state (2+) of its respective iron centers ( $[\text{PhBP}_3] = \text{PhB}(\text{CH}_2\text{PPh}_2)_3$ ).<sup>1,2</sup> Because molecular nitride species might be intermediates of N<sub>2</sub> reduction schemes,<sup>3</sup> an avenue of interest was to examine its reactivity toward proton sources<sup>1</sup> and molecular hydrogen.<sup>4</sup> In the latter context, molecular iron nitrides, whether bridging or terminal, are not known to react with H<sub>2</sub>, despite the proposition that such reactions are mechanistically important during the Haber–Bosch ammonia synthesis process.<sup>5</sup> Herein, we establish the facile heterolysis of H<sub>2</sub> under mild conditions (rt, 1 atm H<sub>2</sub>) upon exposure to low-coordinate L<sub>3</sub>Fe<sup>II</sup>-(μ-N)-Fe<sup>II</sup>L<sub>3</sub> and L<sub>3</sub>Fe<sup>III</sup>-(μ-N)-Fe<sup>II</sup>L<sub>3</sub> complexes. The resulting diiron imide–hydride products, L<sub>3</sub>Fe-(μ-NH)(μ-H)-FeL<sub>3</sub>, are structurally unique.<sup>6,7</sup>

The iron μ-nitrides featured in this study are  $\{([\text{PhBP}_3]\text{Fe})_2(\mu\text{-N})\}\{\text{Na}(\text{THF})_5\}$ ,  $\{\mathbf{1}\}^-\{\text{Na}(\text{THF})_5\}$ , a brown complex that consists of two antiferromagnetically coupled high-spin Fe(II) centers,<sup>1</sup> and its neutral one-electron oxidation product, greenish black  $\{([\text{PhBP}_3]\text{Fe})_2(\mu\text{-N})\}$  (**2**). Access to the latter species was predicted by the cyclic voltammogram of  $\{\mathbf{1}\}^-$ , which showed a reversible redox couple at -1.3 V versus Fc<sup>+/0</sup>. Exposure of  $\{\mathbf{1}\}^-$  to numerous oxidants generated varying amounts of the Fe<sup>III</sup>-(μ-N)-Fe<sup>II</sup> species **2**. PCl<sub>3</sub> proved synthetically most reliable in this regard and eliminated NaCl and Cl<sub>2</sub>P–PCl<sub>2</sub> as byproducts to afford **2** in 66% crystallized yield. Because the reported structure of  $\{\mathbf{1}\}^-$  exhibited an unexpectedly bent Fe–N–Fe linkage and also experienced modest disorder about the N-atom,<sup>1</sup> we undertook the X-ray characterization of single crystals of **2** for comparison. Its core structure is shown in Figure 1 (top).<sup>8</sup> The Fe–N bond distances of 1.668(2) and 1.683(2) Å for **2** are similar to those observed for  $\{\mathbf{1}\}^-$  (Fe–N = 1.675(5) and 1.705(5) Å). The Fe–N–Fe linkage exhibits an even more pronounced bend (142.4(1)°) than that for the case of  $\{\mathbf{1}\}^-$ . An interesting contrast to the structure of  $\{\mathbf{1}\}^-$  is that there is substantial asymmetry about the Fe–P bonds of **2**, perhaps due to a Jahn–Teller distortion that results from placement of one unpaired electron in a nearly degenerate π-orbital set. Specifically, Fe1 exhibits two long and one short Fe–P bond, and Fe2 exhibits two short and one long Fe–P bond. A rhombic signal consistent with the *S* = 1/2 ground state of **2** was observed in its 4 K X-band EPR spectrum.<sup>9</sup> The low-energy charge transfer and d–d transitions apparent in the optical spectrum of  $\{\mathbf{1}\}^-$  appear to be blue-shifted in the spectrum of **2** owing to its higher oxidation state. Also, its solid-state SQUID magnetization data are most consistent with an antiferromagnetically coupled Fe<sup>II</sup>Fe<sup>III</sup> spin system. The magnetic moment of **2** increased from 1.82 μ<sub>B</sub> at 4 K to 3.40 μ<sub>B</sub> at 300 K, most likely indicative of a ground state doublet with thermally accessible higher spin states.

Chemical confirmation of the μ-nitride functionality of **2** was afforded upon its exposure to an atmosphere of CO, which rapidly and quantitatively produced equimolar amounts of the previously

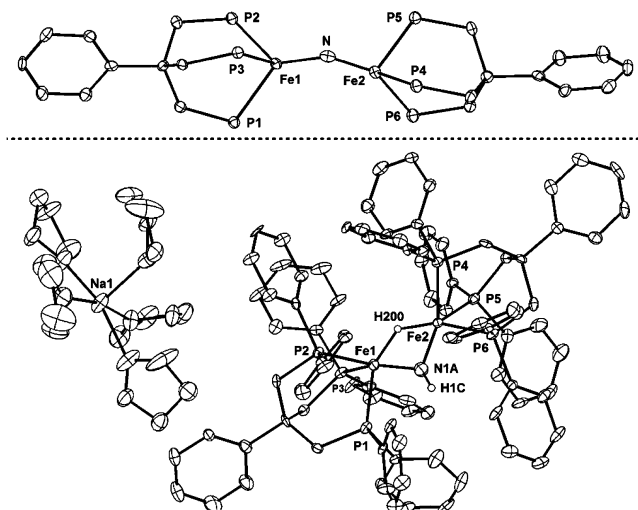
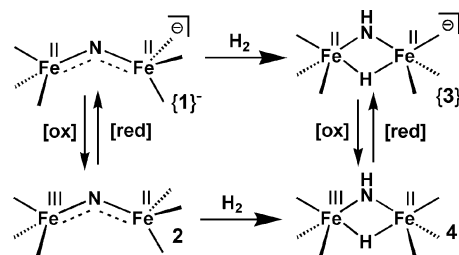
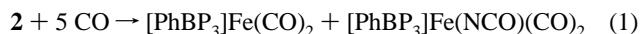


**Figure 1.** (Top) Solid-state molecular structure of  $([\text{PhBP}_3]\text{Fe})_2\text{N}$  (**2**) with phosphino phenyl groups and two THF solvent molecules removed for clarity. Selected bond lengths (Å) and angles (°): Fe1–N, 1.683(2); Fe2–N, 1.668(2); Fe1–N–Fe2, 142.4(1). (Bottom) Solid-state molecular structure of  $[(\text{PhBP}_3)\text{Fe}_2(\mu\text{-NH})(\mu\text{-H})][\text{Na}(\text{THF})_5]$  (**3**). Selected bond lengths (Å) and angles (°): Fe1–N1A, 1.826(5); Fe2–N1A, 1.790(5); Fe1–Fe2, 2.6595(9); Fe1–N1A–Fe2, 94.7(3).

### Scheme 1



characterized complexes  $[\text{PhBP}_3]\text{Fe}(\text{CO})_2$ <sup>10</sup> and  $[\text{PhBP}_3]\text{Fe}(\text{NCO})(\text{CO})_2$  (NCO):<sup>1</sup>



Exposure of a brown THF solution of  $\{\mathbf{1}\}^-\{\text{Na}(\text{THF})_5\}$  to an atmosphere of H<sub>2</sub> at room temperature resulted in a color change to green within minutes. Isolation and characterization of the resulting product after 2 h demonstrated a net 1,2 H–H addition across the Fe–N–Fe linkage to produce the bridged species  $[(\text{PhBP}_3)\text{Fe}_2(\mu\text{-NH})(\mu\text{-H})][\text{Na}(\text{THF})_5]$  (**3**) ( $\{\mathbf{3}\}^-\{\text{Na}(\text{THF})_5\}$ ) (Scheme 1). The absence of low-energy d–d transitions in the optical spectrum of  $\{\mathbf{3}\}^-$  intimated a low-spin diamagnetic system—plausible given the presence of two five-coordinate Fe(II) centers supported by strong-field ligands. Complex  $\{\mathbf{3}\}^-$  is indeed diamagnetic and was conveniently characterized by <sup>1</sup>H, <sup>31</sup>P, and <sup>15</sup>N

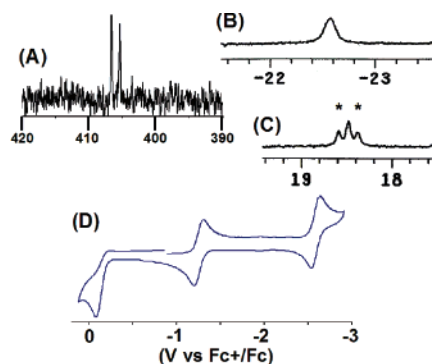


**Figure 2.** (A) Proton-coupled  $^{15}\text{N}$  NMR spectrum, (B)  $\mu\text{-H}$  resonance observed in the  $^1\text{H}$  NMR spectrum, and (C)  $\mu\text{-NH}$  resonance observed in the  $^1\text{H}$  NMR spectrum of  $\{3\}^-$  (50%  $^{15}\text{N}$ ). Peaks marked with an asterisk are due to coupling with the  $^{15}\text{N}$  nucleus. (D) Cyclic voltammetry of  $\{3\}^-$  [ $\text{Na}(\text{THF})_5$ ] in THF (0.3 M [TBA][PF $_6$ ], 50 mV/s).

NMR spectroscopies. Its  $^{31}\text{P}$  NMR spectrum exhibited a singlet resonance at  $\delta$  66 ppm, and its  $^1\text{H}$  NMR spectrum featured diagnostic resonances at  $\delta$  +18.5 and  $-22.4$  ppm for the  $\mu\text{-NH}$  and  $\mu\text{-H}$  ligands, respectively. These resonances were absent in the  $^1\text{H}$  NMR spectrum when  $\{1\}^-$  was hydrogenated under  $\text{D}_2$ .  $^{15}\text{N}$ -labeled  $\{3\}^-$  (50%  $^{15}\text{N}$ ) was prepared by the hydrogenation of  $\{1\}^-$  (50%  $^{15}\text{N}$ ) and featured a doublet at  $\delta$  406 ppm ( $J_{\text{N-H}} = 63$  Hz; Figure 2), shifted significantly upfield from the  $^{15}\text{N}$  resonance of its precursor  $\{1\}^-$  ( $\delta = 801$  ppm (s)).<sup>1</sup> Additionally, the  $\text{NH}$  resonance at  $\delta$  +18.5 ppm in the  $^1\text{H}$  NMR spectrum of  $\{3\}^-$  (50%  $^{15}\text{N}$ ) exhibited a doublet superimposed on a singlet, resulting from coupling to the 50%  $^{15}\text{N}$  label (Figure 2). We were surprised to find that vibrations associated with the imide and hydride ligands could not be observed in the IR spectrum of  $\{3\}^-$ , regardless of how the samples were prepared (THF/KBr solution, KBr pellet, Nujol).

The cyclic voltammetry of  $\{3\}^-$  (Figure 2) demonstrated an irreversible oxidative process at  $-0.15$  V and two low-potential redox events at  $-1.25$  and  $-2.58$  V versus  $\text{Fc}^+/\text{Fc}$ . The reversible event at  $-1.25$  V is indicative of an  $\text{Fe}^{\text{III}}\text{Fe}^{\text{II}}/\text{Fe}^{\text{II}}\text{Fe}^{\text{II}}$  redox couple akin to that observed for  $\{1\}^-$ . This suggests that the hydrogenation of neutral **2** might lead to a stable neutral imide hydride. In fact, exposure of green **2** to an atmosphere of hydrogen generated neutral  $\{[(\text{PhBP}_3)\text{Fe}]_2(\mu\text{-NH})(\mu\text{-H})\}$  (**4**). This product could be alternatively generated by the oxidation of  $\{3\}^-$  with  $[\text{NO}][\text{PF}_6]$ . The lower-potential, pseudo-reversible couple observed in the cyclic voltammogram of  $\{3\}^-$  at  $-2.6$  V presumably constitutes an  $\text{Fe}^{\text{II}}(\mu\text{-NH})(\mu\text{-H})\text{Fe}^{\text{II}}/\text{Fe}^{\text{II}}(\mu\text{-NH})(\mu\text{-H})\text{Fe}^{\text{I}}$  redox process. Electrochemical access to the reduced  $\text{Fe}^{\text{II}}\text{Fe}^{\text{I}}$  species is noteworthy given the recent interest in  $\text{Fe}^{\text{II}}\text{Fe}^{\text{I}}$  bimetallic diiron hydride cores as possible intermediates of biological  $\text{H}_2$  production.<sup>11</sup>

The 4 K X-band EPR spectrum of **4** featured the anticipated axial signal for an  $S = 1/2$  electronic configuration. The absence of a low-field signal in the spectrum was suggestive of the presence of two low-spin iron centers. Delocalization of its single unpaired electron over both metals was implied by weak phosphorus coupling in the  $g_{\perp}$  region arising from all six phosphorus nuclei (simulation provided  $A_x = 12$  G). As for its nitride precursor **2**, solid-state SQUID magnetization data for **4** confirmed the presence of one unpaired electron at low temperature ( $\mu_{\text{eff}} = 2.12 \mu_{\text{B}}$  at 4 K). We were surprised to find that the moment increased as the temperature was raised to a value of  $3.30 \mu_{\text{B}}$  at 300 K, again likely indicating low-lying excited states despite the presumed strong field nature of the system. Distinct from  $\{3\}^-$ , a readily discernible vibration for the  $\text{NH}$  ligand (IR; Nujol mull) could be observed at  $3319 \text{ cm}^{-1}$  for **4**.

Crystals of  $\{3\}^-$  suitable for XRD analysis were obtained (Figure 1 (bottom)). The bridging ligands are disordered over two positions as a result of the  $\text{NH}$  and  $\text{H}$  ligands alternating positions randomly throughout the crystal. However, electron density attributable to both the imide hydrogen and the hydride ligand could be located in the difference map, and the data were satisfactorily refined when the  $\text{Fe-H}$  distances were constrained to be equal. The solution was of sufficient quality to unequivocally establish the connectivity of the diiron core and to provide reliable structural data concerning the statistically more prevalent  $\text{Fe}-(\mu\text{-NH})-\text{Fe}$  linkage (ca. 70% occupancy). In comparison with nitride  $\{1\}^-$ , the  $\text{Fe-N}$  bond lengths for  $\{3\}^-$  are expanded by an average distance of  $0.118 \text{ \AA}$  ( $\text{Fe-N} = 1.790(5)$  and  $1.826(5) \text{ \AA}$  for  $\{3\}^-$ ). Also, the  $\text{Fe-N-Fe}$  bond angle exhibits a severe contraction from  $135.9(3)$  to  $94.7(3)^\circ$  upon installation of the bridging hydride ligand. The  $\text{Fe-Fe}$  distance of  $2.6588(9) \text{ \AA}$  observed for  $\{3\}^-$  is approximately  $0.45 \text{ \AA}$  shorter than that of  $\{1\}^-$  and is similar to the  $\text{Fe-Fe}$  distances observed in hydrogenase model compounds for which direct iron-iron interactions have been implicated.<sup>12</sup> Our attempts to obtain reliable structural parameters for **4** have been frustrated thus far by severe disorder problems in the crystals we have examined.

In summary, low-valent and low-coordinate bridging iron nitrides stabilized by  $[\text{PhBP}_3]$  ligands mediate facile  $\text{H}_2$  activation under mild conditions (room temperature, 1 atm  $\text{H}_2$ ). In contrast to previous work from our lab concerning the hydrogenation of low-spin  $\text{Fe}(\text{III})$  imides,<sup>4a</sup> complete scission of the  $\text{Fe-N}$  linkage is not observed. This is presumably due to the presence of an additional metal center that traps the imide-hydride as a bimetallic species.

**Acknowledgment.** We thank the NIH for financial support (GM-070757 to J.C.P., GM-072291 to M.P.M.), and Dr. Angel J. Di Bilio, Lawrence Henling, and Dr. Michael W. Day for assistance.

**Supporting Information Available:** Experimental and characterization data; crystallographic data. This material is available free of charge via the Internet at <http://pubs.acs.org>.

## References

- (1) Brown, S. B.; Peters, J. C. *J. Am. Chem. Soc.* **2005**, *127*, 1913.
- (2) For some examples of structurally characterized  $\text{Fe}-(\mu\text{-N})-\text{Fe}$  linkages, see: (a) Jüstel, T.; Müller, M.; Weyhermüller, T.; Kressl, C.; Bill, E.; Hildebrandt, P.; Lengen, M.; Grodzicki, M.; Trautwein, A. X.; Nuber, B.; Wieghardt, K. *Chem.-Eur. J.* **1999**, *5*, 793. (b) Scheidt, W. R.; Summerville, D. A.; Cohen, I. A. *J. Am. Chem. Soc.* **1976**, *98*, 6623.
- (3) (a) Chatt, J.; Dilworth, J. R.; Richards, R. L. *Chem. Rev.* **1978**, *78*, 589. (b) Buhr, J. D.; Taube, H. *Inorg. Chem.* **1979**, *18*, 2208. (c) Yandulov, D. V.; Schrock, R. R. *Science* **2003**, *301*, 76. (d) Betley, T. A.; Peters, J. C. *J. Am. Chem. Soc.* **2004**, *126*, 6252.
- (4) For examples of  $\text{H}_2$  addition to metal-imide-type linkages, see: (a) Brown, S. B.; Peters, J. C. *J. Am. Chem. Soc.* **2004**, *126*, 4539. (b) Cummins, C. C.; Baxter, S. M.; Wolczanski, P. T. *J. Am. Chem. Soc.* **1988**, *110*, 8731. (c) Pool, J. A.; Lobkovsky, E.; Chirik, P. J. *Nature* **2004**, *427*, 527.
- (5) Ertl, G. *Chem. Rev.* **2001**, *1*, 33.
- (6) The  $\mu\text{-NH}$  ligand is uncommon. For several structurally related examples, see: (a) Armor, J. N. *Inorg. Chem.* **1978**, *17*, 203. (b) Shaver, M. P.; Fryzuk, M. D. *J. Am. Chem. Soc.* **2005**, *127*, 500. (c) Roesky, H. W.; Bai, Y.; Noltemeyer, M. *Angew. Chem., Int. Ed.* **1989**, *28*, 754.
- (7) ENDOR detection of a paramagnetic iron hydride species formed within the nitrogenase cofactor has been recently reported: Igarashi, R. Y.; Laryukhin, M.; Dos Santos, P. C.; Lee, H. I.; Dean, D. R.; Seefeldt, L. C.; Hoffman, B. M. *J. Am. Chem. Soc.* **2005**, *127*, 6231.
- (8) Complete structural details for **2** and  $\{3\}^-$  [ $\text{Na}(\text{THF})_5$ ] can be found in the Supporting Information.
- (9) EPR and SQUID magnetization data for **2** and **4**, and optical data for all species, can be found in the Supporting Information.
- (10) Brown, S. B.; Peters, J. C. *J. Am. Chem. Soc.* **2003**, *125*, 322.
- (11) (a) Razavet, M.; Borg, S. J.; George, S. J.; Best, S. P.; Fairhurst, S. A.; Pickett, C. J. *Chem. Commun.* **2002**, 700. (b) Darensbourg, M. Y.; Lyon, E. J.; Zhao, X.; Georgakaki, I. P. *Proc. Natl. Acad. Sci. U.S.A.* **2003**, *100*, 3683.
- (12) (a) Peters, J. W.; Lanzilotta, W. N.; Lemon, B. J.; Seefeldt, L. C. *Science* **1998**, *282*, 1853. (b) Georgakaki, I. P.; Thomson, L. M.; Lyon, E. J.; Hall, M. B.; Darensbourg, M. Y. *Coord. Chem. Rev.* **2003**, *238*, 255. (c) Gloaguen, F.; Lawrence, J. D.; Schmidt, M.; Wilson, S. R.; Rauchfuss, T. B. *J. Am. Chem. Soc.* **2001**, *123*, 12518.

JA0544509